Electronic Supplementary Information

Interfacial interaction induced OER activity of MOF derived superhydrophilic Co_3O_4-NiO hybrid nanostructures

Ashish Gaur,[a] Vikas Pundir,[a] Krishankant,[a] Ritu Rai,[a] Baljeet Kaur,[a] TakahiroMaruyama,[b] ChandanBera,[a] and Vivek Bagchi[a]*

[a] *Institute of Nano Science and Technology (INST) Sector-81, Knowledge City, Sahibzada Ajit Singh Nagar, Punjab, Pin - 140306.*

[b] *Department of Applied Chemistry, Meijo University, 1-501 Shiogamaguchi, Tempaku, Nagoya 468-8502, Japan.*

*Corresponding author: vivekbagchi@gmail.com, bagchiv@inst.ac.in

S1. Experimental section

S2.1.PXRD spectra of Co_3O_4 and bare NF

S2.2.PXRD spectra of MOF over NF

S3.1.SEM images of MOF over NF

S3.2. SEMimages of NiO/NF

S4.TEM and HRTEM analysis of Co_3O_4

S5.1.Comparison of the XPS peak position of Co 2p and Ni 2p in different catalysts.

S5.2.Wide scan XPS spectrum of Co_3O_4

S5.3.High resolution XPS spectrum of Co 2p and O 1s of individual Co_3O_4

S5.4. Deconvoluted peak parameters of the XPS analysis of Co_3O_4-NiO/NF

S5.5. Deconvoluted peak parameters of the XPS analysis of Co_3O_4

S6.1. OER scheme showing the mechanism .

S6.2 Mass loading of all the catalysts over Nickel foam.

S6.3. LSV plot of $NiCo_2O_4$-NiO/NF and Co_3O_4-NiO/NF

S6.4 Comparative table of OER performance of recently reported $Co_3O_4$and NiO based electrocatalyst.

S6.5. ECSA normalized LSV curve of Co_3O_4-NiO/NF

S6.6. CV of all the catalysts for C_{dl} calculations

S6.7.PXRD spectra of the catalyst after durability test

S6.8.HRTEM analysis of catalyst after durability test

S6.9.STEM elemental mapping of catalyst after durability test

S6.10 XPS analysis of catalyst after stability

S7. Theoretical studies

S1 Experimental procedure

Synthesis of Co_3O_4: Co_3O_4 nanoparticles were synthesized by using metal organic framework as a precursor ($Co_2(OH)_2(BDC)$)The synthesis of MOF is done by using previously reported method [1] with slight modification in which 2 mmol of $Co(NO_3)_2.6H_2O$, and 2 mmol of 1,4-benzenedicarboxylic acid (H_2BDC). Firstly the 2 mmol of 1,4-benzenedicarboxylic acid (H_2BDC) were dissolve in 10 mL of N,N-dimethylformamide (DMF) then 1 mL of 0.5 M NaOH solution was added under continuous stirring. In other flask 2 mmol of $Co(NO_3)_2.6H_2O$ were dissolve in 10 mL of N,N-dimethylformamide (DMF). Both the solutions were mixed together in the 50 mL Teflon-lined stainless steel autoclave and the autoclave was heated was heated for 20 h at 110°C temperature. The as obtained $Co_2(OH)_2(BDC)$ MOF was washed three times with DMF and ethanol and dried naturally. The as obtained MOF was heated in furnace at 500°C for 3 hr at a ramp rate of 5°C/min. After annealing Co_3O_4 were obtained and used as it is.

Synthesis of NiO/NF: The NiO/NF electrode was obtained by heating the bare nickel foam at 500°C for 3 hr at a ramp rate of 5°C /min. After annealing the NiO nanostructures were formed over nickel foam.

S2.1.PXRD spectra ofCo_3O_4 and bare NF

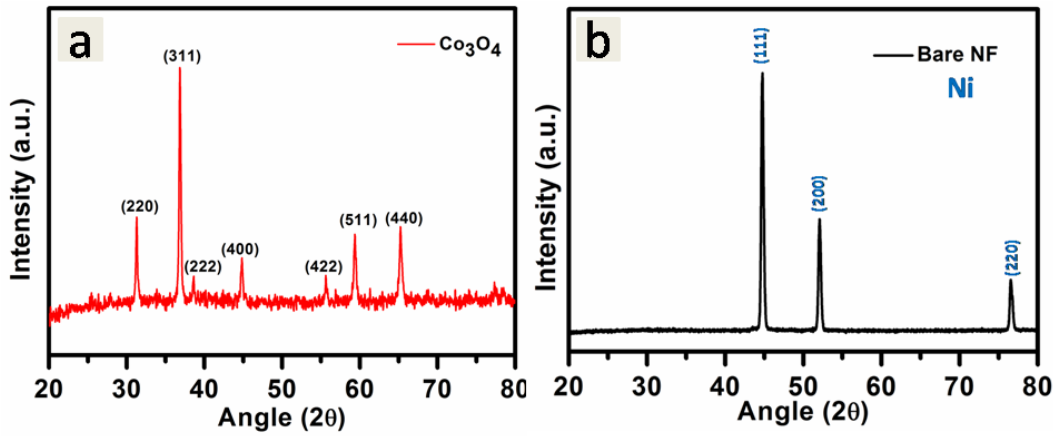

Figure S1 PXRD spectrum of Co_3O_4 (a) and NiO/NF (b) showing the presence of all the respective peaks

The XRD pattern was obtained in the 2θ angular region of 20° to 80° with an increment of 0.00190/Step.

S2.2. PXRD spectra of MOF over NF

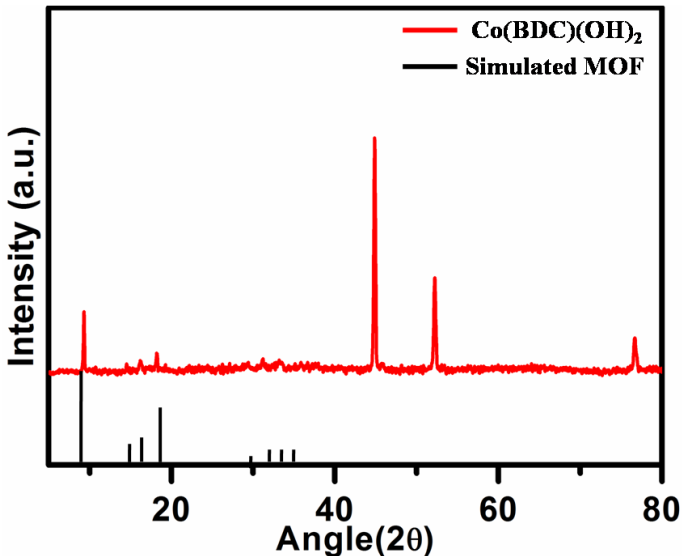

Figure S2PXRD spectra of MOF over NF overlapped with the simulated MOF

S3.1.SEM images of MOF over NF

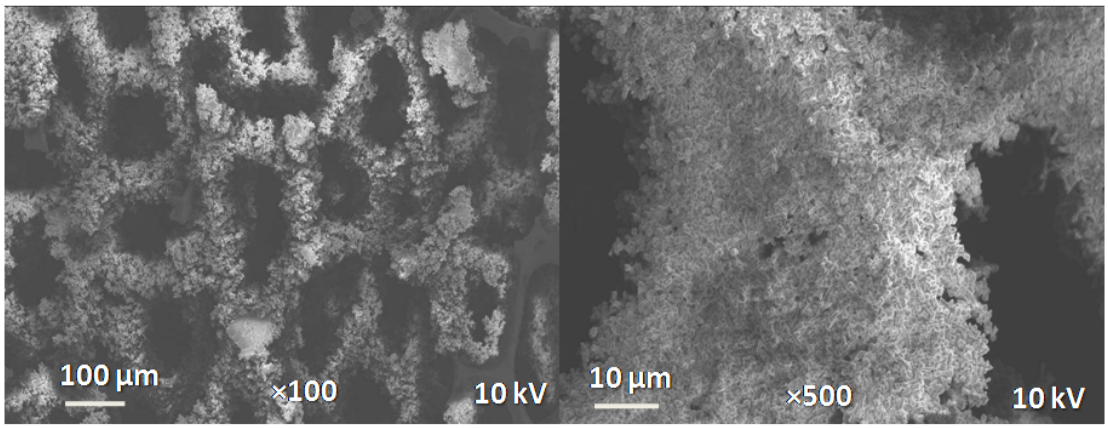

Figure S3. SEM images of MOF over NF

S3.2. SEM images of NiO over NF

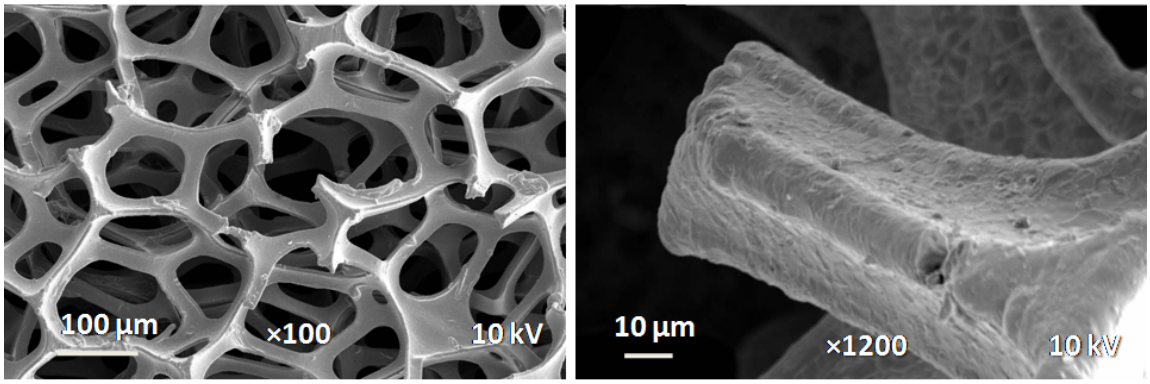

Figure S4. SEM images of NiO formed over NF at different magnification

S4. TEM and HRTEM images of Co_3O_4 nanoparticles

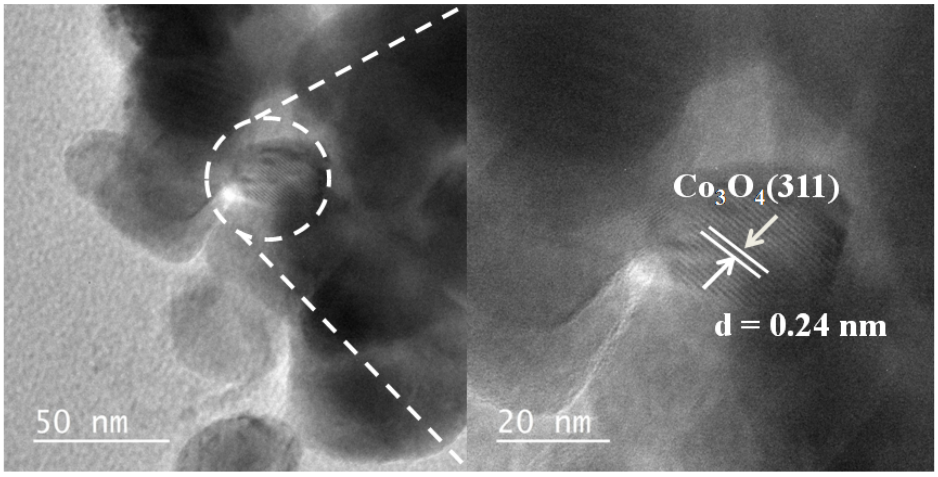

Figure S5. (a) TEM and (b) HRTEM images of individual Co_3O_4 nanoparticles with the corresponding plane and d spacing value

S5.1.Comparison of the XPS peak position of Co 2p and Ni 2p in different catalysts.

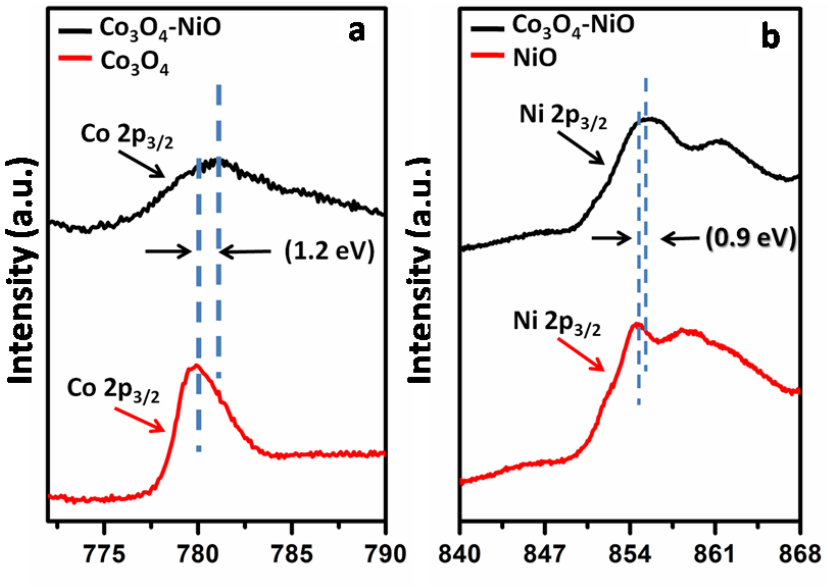

Figure S6 (a)High resolution $Co2p_{3/2}$ XPS spectra of Co_3O_4-NiO and Co_3O_4 (b) high resolution XPS Ni 2p spectra of Co_3O_4-NiO and NiO

S5.2 Wide scan XPS spectra of Co_3O_4

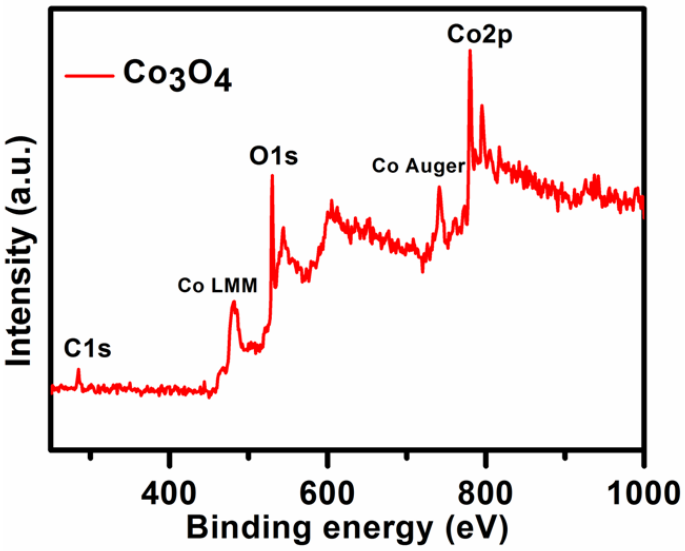

Figure S7 Wide scan XPS spectra of individual Co_3O_4

S5.3. XPS spectra of Co_3O_4

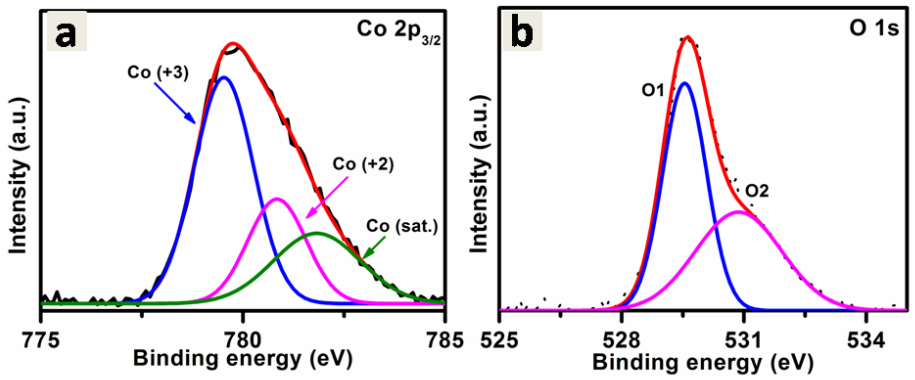

Figure S8 (a) High resolution XPS spectra of Co2p present in Co_3O_4**(b)**The deconvoluted XPS spectra of O1s present in Co_3O_4

S5.4. Table containing the various parameters obtained after the deconvolution of XPS spectra of Co_3O_4-NiO/NF

Element	Peak	BE (eV)	FWHM	Area (%)
Co 2p	Co^{3+} Co^{2+} Sat.	779.6 781.3 781.8	2.04 2.11 5.67	52.49 24.10 23.40
Ni 2p	Ni^{+2} Ni^{+3} Sat.	853.7 & 871.7 855.5 & 874.3 861.0	1.49 & 2.6 2.8 & 4.8 5.1	10.1 & 9.9 30.7 & 17.9 31.2
O 1s	O1 O2	529.4 531.0	1.21 2.89	34.6 65.3

Table S1 Table containing the deconvoluted peak parameters of Co_3O_4– NiO/NF obtained after the XPS analysis

S5.5. Table containing the various parameters obtained after the deconvolution of XPS spectra of Co_3O_4

Element	Peak	BE (eV)	FWHM	Area (%)
Co 2p	Co^{3+} Co^{2+} Sat.	778.8 779.6 780.9	1.72 1.69 2.54	52.33 23.7 23.9
O 1s	O1 O2	529.5 530.8	1.27 2.48	54.2 45.7

Table S2 Table containing the deconvoluted peak parameters of Co_3O_4 obtained after the XPS analysis

S6.1. Scheme showing mechanism for electrocatalytic oxygen evolution

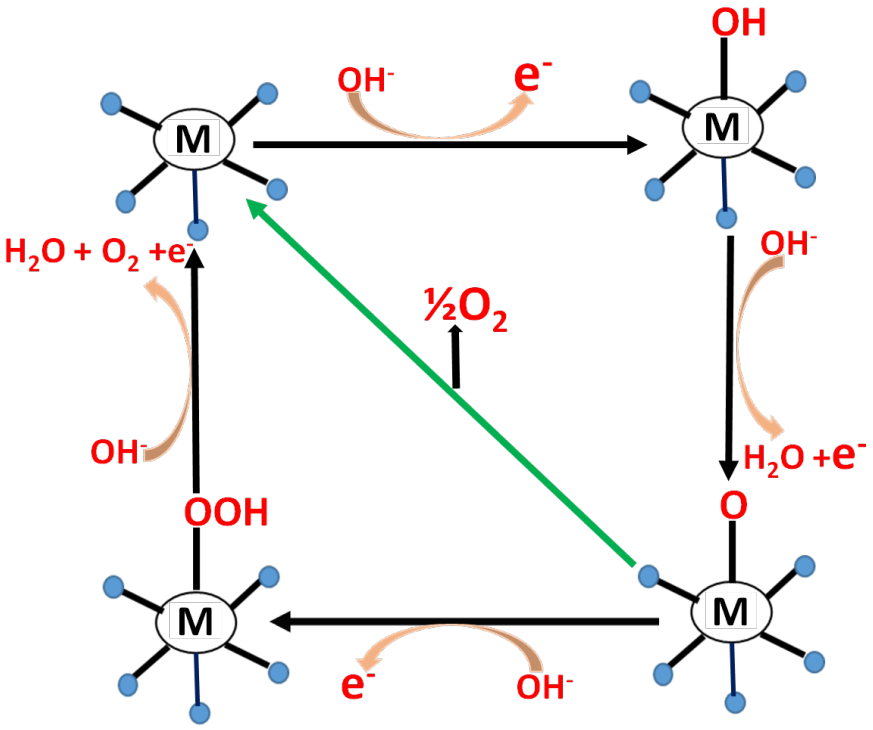

Figure S9 scheme showing the oxygen evolution reaction on metal center.

S6.2. Mass loading of all the catalyst on nickel foam.

Catalyst	Mass loading (mg cm^{-2})
Co_3O_4-NiO/NF	3.35
Co_3O_4/NF	3.35
NiO/NF	1.4
RuO_2/NF	3.35

Table S3 Mass loading of all the catalyst over NF

S6.3. Comparison of OER activity of the $NiCo_2O_4$-NiO/NF and Co_3O_4-NiO/NF

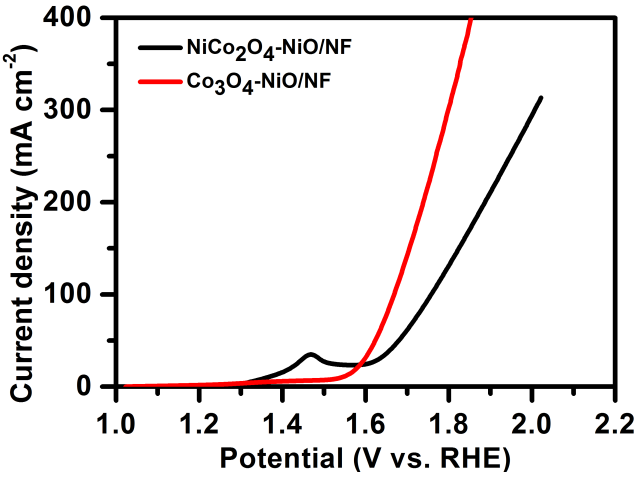

Figure S10 LSV curve of $NiCo_2O_4$-NiO/NF and Co_3O_4-NiO/NF

S6.4 Comparative table of the electrochemical activity of previously reported $Co_3O_4$and NiObased catalyst

Material	Electrolyte	Substrate	Overpotential (10 mA cm^{-2})	Tafel slope (mV/dec)	Reference
Co_3O_4 nanoparticle	1 M KOH	GCE	350	84	2
Co_3O_4@GF_KMnO4	0.1M KOH	RDE	440	60.3	3
Co_3O_4-200	1 M KOH	GCE	390	59.2	4
$Co3O_4$@C	1 M KOH	CP	310	69	5
Co_3O_4/LIG	0.1 KOH	RRD	340	40	6
NiOx/$NiCo_2O_4$/$Co3O_4$	1M NaOH	Nickel sheet	315	76	7
Co_3O_4 nanowires	1M KOH	GCE	405	72	8
M-Co_3O_4	1M KOH	GCE	370	89	9
rGO-Co_3O_4	1M KOH	RDE	410	85	10
Co_3O_4/$NiCo_2O_4$	1M KOH	NF	340	88	11
Porous Co_3O_4	1M KOH	RDE	368	59	12
Co_3O_4 nanocubes	1M KOH	GCE	402	67	13
Co_3O_4-C	1M KOH	NF	310	90	14
Ultrathin Co_3O_4	1M KOH	RDE	307	76	15
NiO-400	1M NaOH	SS	530	136.7	16
Ni-$C_{500\text{-}20}$	1M KOH	CP	353	97	17
Ni/NiO@rGO	0.5M KOH	GCE	480	41	18

NiO-300	1M KOH	GCE	370	156	19
NiO/NiS	1M KOH	NF	209	60	20
NiCoON/NF	1M KOH	NF	247	35	21
$Ni_4(PET)_8$	1M KOH	GCE	280	60	22
Coo-Cal	1M KOH	GCE	306	67	23
Co_3O_4-NiO/NF	**1M KOH**		**311**	**90**	**This work**

Table S4 Comparative table of electrochemical properties of recently reported $Co_3O_4$and NiObased electrocatalyst.

S6.5. ECSA normalized LSV curve of Co_3O_4-NiO/NF

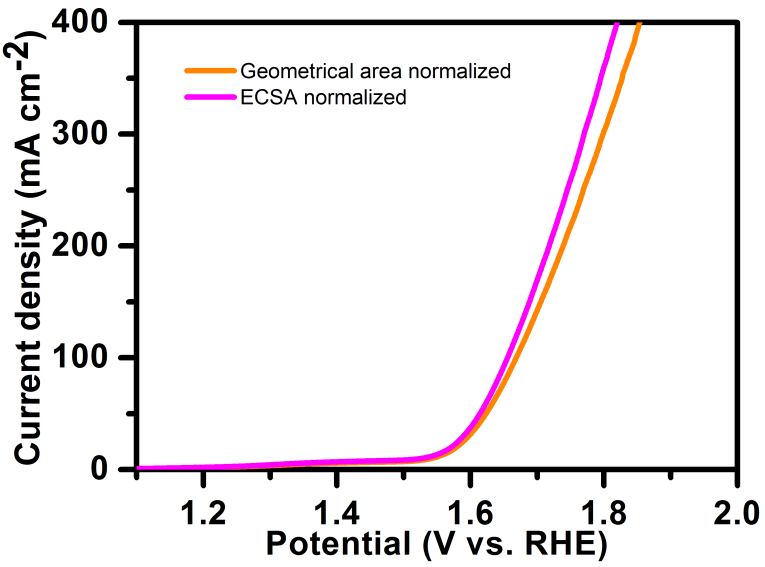

Figure S11 Geometrical area normalized and ECSA normalized OER activity of Co_3O_4-NiO/NF catalyst

S6.6. Cyclic voltammetry curve of Co_3O_4-NiO , Co_3O_4 and NiO

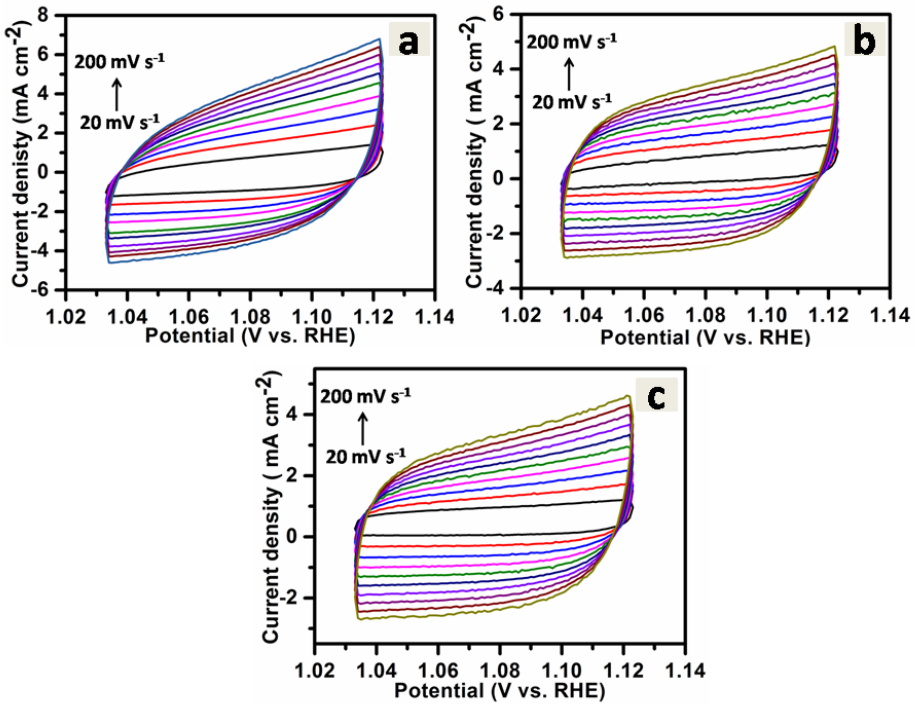

Figure S12 Cyclic voltammetry curve of (a)Co_3O_4-NiO/NF, (b) Co_3O_4/NF and (c) NiO/NF for the calculation of C_{dl}

S6.7.PXRD spectra of the catalyst after durability test

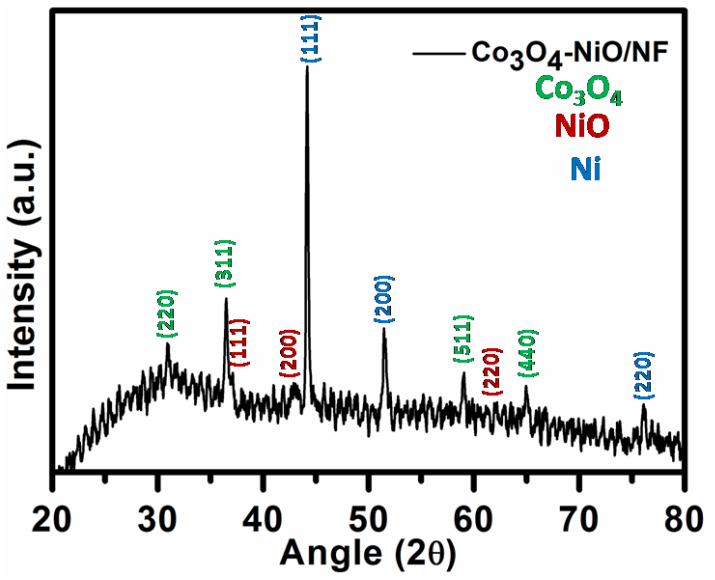

Figure S13 PXRD spectra of the catalyst after stability showing the retention of all the phases present

S6.8. HRTEM analysis of catalyst after durability test

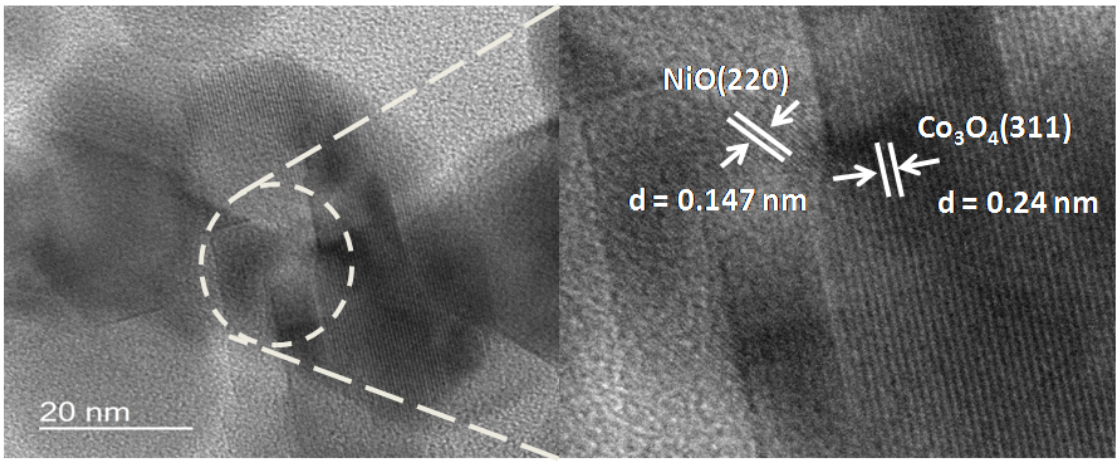

Figure S14 HRTEM analysis of the catalyst after stability

S6.9. STEM elemental mapping of catalyst after durability test

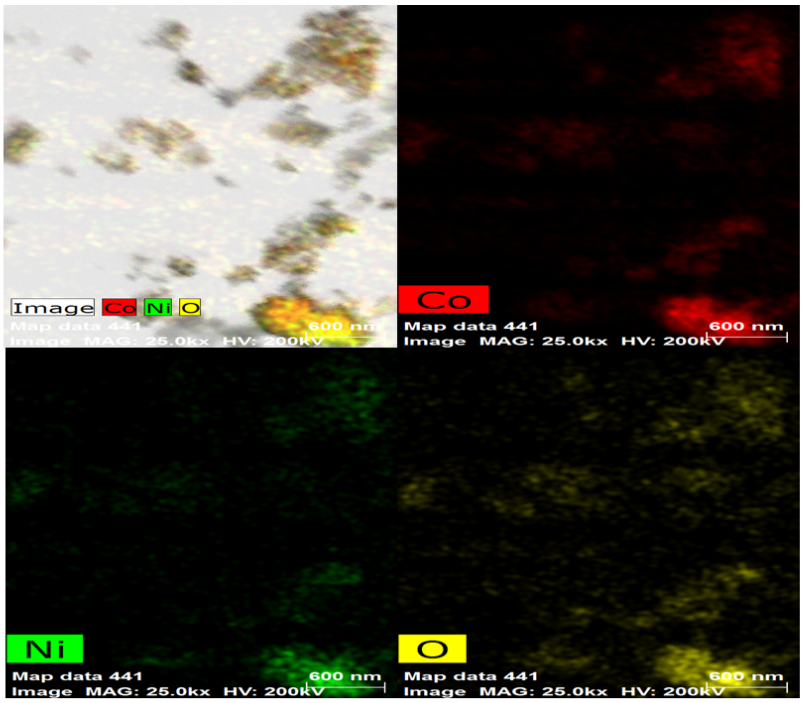

Figure S15.STEM elemental mapping of the catalyst showing the presence of all the elements after stability also

S6.10. STEM elemental mapping of catalyst after durability test

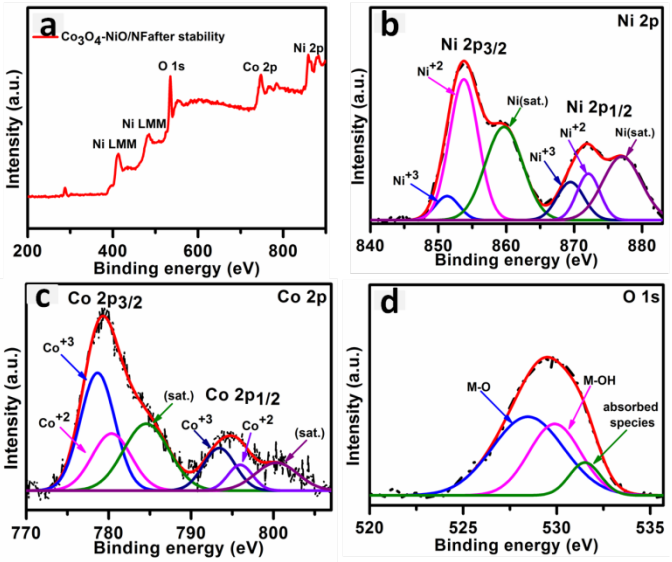

Figure S16 XPS of the Co_3O_4-NiO/NF catalyst after stability (a) survey spectrum of catalyst . HR spectra of (b) Ni 2p, (c) Co 2p and (d) O 1s electron: experimental data (dotted curve) and fitting results (solid curve). The peaks are assigned by oxidation states of different elements with their splitting term

S7 Theoretical details

Density functional theory has been used to simulate theoretical models to observe the different active sites for O* and OH* adsorption on the Co_3O_4-NiO/NF heterostructure. Here, we present the detailed steps to understand the OER mechanism , which is a four electron transfer process.

$$H_2O\ (l) + *\ \leftrightarrow\ OH^* + H^+ + e^- \qquad (1)$$

$$OH\ *\ \leftrightarrow\ O^*\ + H^+ + e^- \qquad (2)$$

$$O^* + H_2O\ (l)\ \leftrightarrow\ OOH^* + H^+ + e^- \qquad (3)$$

$$OOH\ *\ \leftrightarrow\ * + O_2 + H^+ + e^- \qquad (4)$$

where * stands for an active site on the surface of heterostructure. O * , OH * and OOH * are adsorbed intermediates.Gibbs energy determines whether a process will be spontaneous or not. For each step, Gibbs energy can be calculated as

$\Delta G_1 = \Delta G(OH^*) - \Delta G(H_2O) + KT\ln a_{H^+} - eU$

$= E(OH^*) - E(^*) - [E(H_2O) - 1/2E(H_2)] + \Delta ZPE - T\Delta S + KT\ln a_{H^+} - eU$ (5)

$\Delta G_2 = \Delta G(O^*) - \Delta G(OH^*) + KT\ln a_{H^+} - eU$

$= E(O^*) - E(OH^*) + 1/2E(H_2) + \Delta ZPE - T\Delta S + KT\ln a_{H^+} - eU$ (6)

$\Delta G_3 = \Delta G(OOH^*) - \Delta G(O^*) + KT\ln a_{H^+} - eU$

$= E(OOH^*) - E(O^*) - [E(H_2O) - 1/2E(H_2)] + \Delta ZPE - T\Delta S + KT\ln a_{H^+} - eU$ (7)

$\Delta G_4 = \Delta G(^*) + \Delta G(O_2) - \Delta G(OOH^*) + KT\ln a_{H^+} - eU$

$= E(^*) - E(OOH^*) + 4.92 + [2E(H_2O) - 1/2E(H_2)] + \Delta ZPE - T\Delta S + KT\ln a_{H^+} - eU$ (8)

Here, K is Boltzmann constant, a_{H^+} represents the activity of protons, U is the potential at the electrode and e is the charge transferred. At standard conditions(pH= 14, T=298.15 K) and U =1.23,Gibbs energies reduce to

$\Delta G_1 = \Delta G(OH^*) - \Delta G(H_2O)$

$= E(OH^*) - E(^*) - [E(H_2O) - 1/2E(H_2)] + \Delta ZPE - T\Delta S$ (9)

$\Delta G_2 = \Delta G(O^*) - \Delta G(OH^*)$

$= E(O^*) - E(OH^*) + 1/2E(H_2) + \Delta ZPE - T\Delta S$ (10)

There exists a universal scaling relationship between OH* and OOH* ,that is

$$E_{ads}(OOH^*) = E_{ads}(OH^*) + 3.2 \text{ [1]}$$

This means the energy difference between OH* and OOH* is constant and hence,independent of the binding strength to the surface. In terms of free energy, the scaling relationship becomes

$\Delta G_3 = -\Delta G_2 + 3.2$ [1] (11)

The process of electrolysis : H_2O $(l) \rightarrow 1/2O_2$ (g) + H_2(g) requires potential of 4.92 eV. As this process involves 4 steps, the potential required for charge transfer is same for each step and equals to 1.23 eV.

Therefore,Gibbs energy for 4the step can be calculated as

$$\Delta G_4 = 4.92 - (\Delta G_1 + \Delta G_2 + \Delta G_3) \quad (12)$$

Also, $\Delta ZPE - T\Delta S$ is unknown for the adsorption on O* and OH* on the heterostructure and therefore, assumed to be zero. E(*), E(O*), E(OH*), E(H_2O), E(H_2) are the energies calculated using DFT .The calculated adsorption energies of O* and OH* on different surfaces/sites are reported in Table.S1.

Table S5. Enthalpies of adsorbates participating in the OER process

Surface	**Total Energy (in eV)**
H_2O	-14.876580475
H_2	-6.88852316
H	-3.44426158
O_2	-9.27246678
H	-4.63623339
OH	-7.08922806

Table S6. Adsorption energies at different sites

S. No.	**Surface**	**Total energy (eV)**
1.	**Co3O4-NiO+O (Ni-site)**	-725.68981
2.	**Co3O4-NiO+O (Co-site)**	-725.7282
3.	**Co3O4-NiO+OH (Ni-site)**	-730.49719
4.	**Co3O4-NiO+OH (Co-site)**	-730.23927
5.	**Co3O4-NiO+OOH (Ni-site)**	-733.50533
6.	**Co3O4-NiO+OOH (Co-site)**	-733.58578

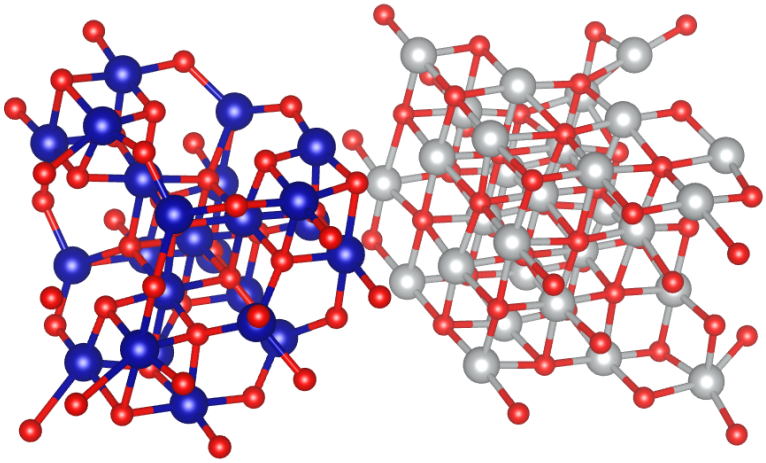

Co_3O_4NiO

Figure S17. Structure of both the individual phases forming heterojunction

References

1. Xue, Z., Liu, K., Liu, Q., Li, Y., Li, M., Su, C.Y., Ogiwara, N., Kobayashi, H., Kitagawa, H., Liu, M. and Li, G., 2019. Missing-linker metal-organic frameworks for oxygen evolution reaction. *Nature communications*, *10*(1), pp.1-8.
2. Liu, S.X., Zhang, R., Lv, W.X., Kong, F.Y. and Wang, W., 2018. Controlled synthesis of Co3O4 electrocatalysts with different morphologies and their application for oxygen evolution reaction. *Int. J. Electrochem. Sci.*, *13*(4), pp.3843-3854.
3. Araújo, M.P., Nunes, M., Rocha, I.M., Pereira, M.F.R. and Freire, C., 2018. Co3O4 nanoparticles anchored on selectively oxidized graphene flakes as bifunctional electrocatalysts for oxygen reactions. *ChemistrySelect*, *3*(35), pp.10064-10076.
4. Tan, P., Wu, Z., Chen, B., Xu, H., Cai, W. and Ni, M., 2019. Exploring oxygen electrocatalytic activity and pseudocapacitive behavior of Co3O4 nanoplates in alkaline solutions. *Electrochimica Acta*, *310*, pp.86-95.
5. Yang, X., Li, H., Lu, A.Y., Min, S., Idriss, Z., Hedhili, M.N., Huang, K.W., Idriss, H. and Li, L.J., 2016. Highly acid-durable carbon coated Co3O4 nanoarrays as efficient oxygen evolution electrocatalysts. *Nano Energy*, *25*, pp.42-50.
6. Ren, M., Zhang, J. and Tour, J.M., 2018. Laser-induced graphene synthesis of Co3O4 in graphene for oxygen electrocatalysis and metal-air batteries. *Carbon*, *139*, pp.880-887.

7. Chen, J., Ling, Y., Lu, Z., Huai, X., Qin, F. and Zhang, Z., 2019. Sandwich-like NiOx/NiCo2O4/Co3O4 nanoflakes enable efficient oxygen evolution electrocatalysis. *Electrochimica Acta*, *322*, p.134753.
8. Wang, Y., Zhou, T., Jiang, K., Da, P., Peng, Z., Tang, J., Kong, B., Cai, W.B., Yang, Z. and Zheng, G., 2014. Reduced mesoporous Co3O4 nanowires as efficient water oxidation electrocatalysts and supercapacitor electrodes. *Advanced Energy Materials*, *4*(16), p.1400696.
9. Sun, H., Zhao, Y., Mølhave, K., Zhang, M. and Zhang, J., 2017. Simultaneous modulation of surface composition, oxygen vacancies and assembly in hierarchical Co 3 O 4 mesoporous nanostructures for lithium storage and electrocatalytic oxygen evolution. *Nanoscale*, *9*(38), pp.14431-14441.
10. Wu, Z., Sun, L.P., Yang, M., Huo, L.H., Zhao, H. and Grenier, J.C., 2016. Facile synthesis and excellent electrochemical performance of reduced graphene oxide–Co 3 O 4 yolk-shell nanocages as a catalyst for oxygen evolution reaction. *Journal of Materials Chemistry A*, *4*(35), pp.13534-13542.
11. Hu, H., Guan, B., Xia, B. and Lou, X.W., 2015. Designed formation of Co3O4/NiCo2O4 double-shelled nanocages with enhanced pseudocapacitive and electrocatalytic properties. *Journal of the American Chemical Society*, *137*(16), pp.5590-5595.
12. Li, Z., Yu, X.Y. and Paik, U., 2016. Facile preparation of porous Co3O4 nanosheets for high-performance lithium ion batteries and oxygen evolution reaction. *Journal of Power Sources*, *310*, pp.41-46.
13. Zhang, P., Han, X., Hu, H., Gui, J., Li, M. and Qiu, J., 2017. In-situ growth of highly uniform and single crystalline Co3O4 nanocubes on graphene for efficient oxygen evolution. *Catalysis Communications*, *88*, pp.81-84.
14. Ren, J.T., Yuan, G.G., Weng, C.C. and Yuan, Z.Y., 2018. Rationally designed Co3O4–C nanowire arrays on Ni foam derived from metal organic framework as reversible oxygen evolution electrodes with enhanced performance for Zn–air batteries. *ACS Sustainable Chemistry & Engineering*, *6*(1), pp.707-718.
15. Li, Y., Li, F.M., Meng, X.Y., Li, S.N., Zeng, J.H. and Chen, Y., 2018. Ultrathin Co3O4 nanomeshes for the oxygen evolution reaction. *Acs Catalysis*, *8*(3), pp.1913-1920.
16. Basharat, F., Rana, U.A., Shahid, M. and Serwar, M., 2015. Heat treatment of electrodeposited NiO films for improved catalytic water oxidation. *RSC advances*, *5*(105), pp.86713-86722.
17. Li, Y., Huang, J., Rao, G., Wu, C., Du, X., Sun, Y., Wang, X. and Yang, C., 2020. Enhanced water oxidation activity of 3D porous carbon by incorporation of heterogeneous Ni/NiO nanoparticles. *Applied Surface Science*, *530*, p.147192.
18. Narwade, S.S., Mali, S.M., Digraskar, R.V., Sapner, V.S. and Sathe, B.R., 2019. Ni/NiO@ rGO as an efficient bifunctional electrocatalyst for enhanced overall water splitting reactions. *International Journal of Hydrogen Energy*, *44*(49), pp.27001-27009.

19. Mondal, A., Paul, A., Srivastava, D.N. and Panda, A.B., 2018. NiO hollow microspheres as efficient bifunctional electrocatalysts for overall water-splitting. *International Journal of Hydrogen Energy*, *43*(47), pp.21665-21674.
20. Khan, N.A., Rashid, N., Junaid, M., Zafar, M.N., Faheem, M. and Ahmad, I., 2019. NiO/NiS heterostructures: an efficient and stable electrocatalyst for oxygen evolution reaction. *ACS Applied Energy Materials*, *2*(5), pp.3587-3594.
21. Li, Y., Hu, L., Zheng, W., Peng, X., Liu, M., Chu, P.K. and Lee, L.Y.S., 2018. Ni/Co-based nanosheet arrays for efficient oxygen evolution reaction. *Nano Energy*, *52*, pp.360-368.
22. Joya, K.S., Sinatra, L., AbdulHalim, L.G., Joshi, C.P., Hedhili, M.N., Bakr, O.M. and Hussain, I., 2016. Atomically monodisperse nickel nanoclusters as highly active electrocatalysts for water oxidation. *Nanoscale*, *8*(18), pp.9695-9703.
23. Xu, W., Lyu, F., Bai, Y., Gao, A., Feng, J., Cai, Z. and Yin, Y., 2018. Porous cobalt oxide nanoplates enriched with oxygen vacancies for oxygen evolution reaction. *Nano Energy*, *43*, pp.110-116.